Quantum Interference between Nonidentical Single Particles

Keyu Su,[1] Yi Zhong,[1] Shanchao Zhang,[1,2] Jianfeng Li,[1,2] Chang-Ling Zou,[3] Yunfei Wang,[1,2,*]
Hui Yan,[1,2,4,†] and Shi-Liang Zhu[1,2,‡]

[1]*Guangdong Provincial Key Laboratory of Quantum Engineering and Quantum Materials,
School of Physics and Telecommunication Engineering, South China Normal University, Guangzhou 510006, China*
[2]*Guangdong-Hong Kong Joint Laboratory of Quantum Matter, Frontier Research Institute for Physics,
South China Normal University, Guangzhou 510006, China*
[3]*CAS Key Laboratory of Quantum Information, University of Science and Technology of China, Hefei 230026, China*
[4]*Guangdong Provincial Engineering Technology Research Center for Quantum Precision Measurement,
South China Normal University, Guangzhou 510006, China*

Quantum interference between identical single particles reveals the intrinsic quantum statistic nature of particles, which could not be interpreted through classical physics. Here, we demonstrate quantum interference between nonidentical bosons using a generalized beam splitter based on a quantum memory. The Hong-Ou-Mandel type interference between single photons and single magnons with high visibility is demonstrated, and the crossover from the bosonic to fermionic quantum statistics is observed by tuning the beam splitter to be non-Hermitian. Moreover, multiparticle interference that simulates the behavior of three fermions by three input photons is realized. Our work extends the understanding of the quantum interference effects and demonstrates a versatile experimental platform for studying and engineering quantum statistics of particles.

Multiparticle quantum interference, such as the well-known Hong-Ou-Mandel (HOM) interference, reveals the quantum statistic nature of particles [1]. There is great research interest in studying the distinct physics of the bosonic and fermionic quantum interference effects [2–5]. The beam splitter (BS) is a fundamental element in conducting quantum interference research. It creates the superposition of particles in different output ports and realizes the interference of amplitudes for particles in each port. Conventionally, the linear BS that separates particles into different spatial modes has been used to demonstrate quantum interference between photons and photons, magnons and magnons, plasmons and plasmons, and even between massive particles (trapped atoms) [6–11]. These demonstrations promise a wide range of potential single-particle level quantum devices for future applications. For instance, quantum interference between single photons provides the single-photon nonlinearity for multiqubit quantum gates [12–14] and thus lies at the heart of quantum information processing and quantum communications [15–17].

Although most of the previous experimental progress has been achieved with identical particles using unitary BS, the principle of quantum interference is not limited to identical particles or Hermitian particle interactions, provided that the coherent superposition between single particles could be realized. Therefore, extending quantum interference to a generalized BS is of fundamental importance. HOM interference between optical photons with different colors has recently been demonstrated with the assistance of a coherent frequency converter [18]. HOM interference between a single magnon excitation and a photonic coherent state has also been demonstrated [19]. In addition, fermionlike quantum interference using a non-Hermitian BS has been observed with identical single photons [20–22] and coherent absorption of the NOON state has been realized [23]. However, for nonidentical particles, it is experimentally challenging to prepare single-particle quantum input for each port and to make them indistinguishable in a beam splitter. Therefore, the quantum interference between genuine nonidentical single particles remains elusive.

In this Letter, the quantum interference between distinct single particles, i.e., single photons and single magnons, is demonstrated for the first time. We construct a hybrid BS for nonidentical particles by realizing coherent quantum conversion between the stored magnon excitation and photons via indistinguishable dark-state polaritons in a cold atom quantum memory. In contrast to the conventional linear BS, our hybrid BS for nonidentical particles could be either Hermitian or non-Hermitian, controllable by an external control laser field. Therefore, our versatile hybrid BS demonstrates the crossover from bosonic bunching statistics [the second-order cross-correlation function $g^{(2)}(0) = 0.40$] to fermionic antibunching statistics [$g^{(2)}(0) = 1.71$], even though the input nonidentical particles are bosons. Furthermore, quantum interference can be extended to more than two particles, with three single photons engineered to
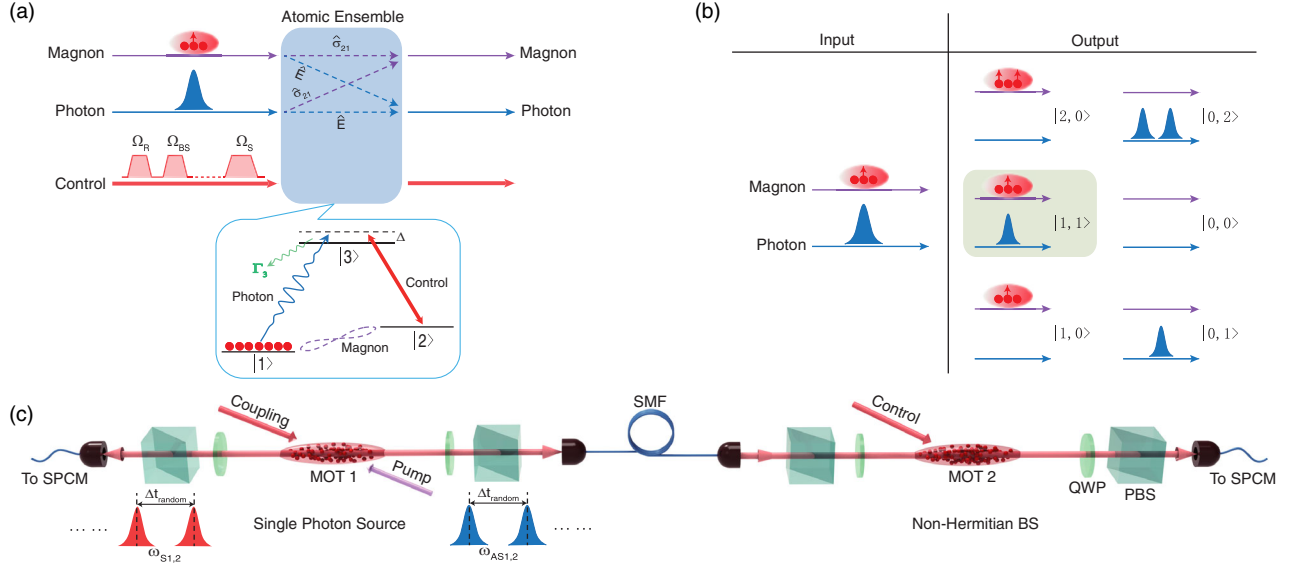
FIG. 1.   Theoretical and experimental schemes. (a) The theoretical scheme of the magnon-photon HOM interferometer. The magnon ($\hat{\sigma}$) and photon ($\hat{E}$) are both in the form of a dark-state polariton (DSP) in an electromagnetically induced transparency (EIT) medium. The red line above the control laser shows the experimental timing sequences: storage of a magnon (Ω_S), interference between two DSPs (Ω_{BS}) and reading out of the magnon (Ω_R). The insert is a Λ-type EIT energy diagram: $|1\rangle = |5S_{1/2}, F = 2, m_F = 2\rangle$, $|2\rangle = |5S_{1/2}, F = 3, m_F = 2\rangle$, $|3\rangle = |5P_{1/2}, F = 3, m_F = 3\rangle$, Γ_3 is the spontaneous decay rate of $|3\rangle$, and Δ is single photon detuning. (b) The input and output states of the magnon-photon HOM interferometer. (c) Experimental setup. MOT$_1$ is a single photon source. The detection of a Stokes photon (ω_{Si}) heralded the generation of an anti-Stokes photon (ω_{ASi}). MOT$_2$ is the non-Hermitian beam splitter. PBS, polarization beam splitter; QWP, quarter wave plate; SPCM, single photon counting module; SMF, single mode fiber.

behave as three fermions by non-Hermitian hybrid BSs. Our work unambiguously demonstrates tunable quantum interference between nonidentical single bosons, which provides a new tool for engineering quantum states for hybrid quantum systems.

Figure 1 schematically illustrates the principle and experimental setup for demonstrating quantum interference between single photons and single magnons. In a cold atom ensemble [Fig. 1(a)], quantum memory could be realized by using an electromagnetically induced transparency (EIT) scheme, by which a control laser could stimulate the coherent conversion between a single flying carrier (photon) and a single collective atomic excitation (magnon) [24–28]. Through such a process, the superposition of the photon and magnon could be realized, and quantum interference between these two distinct bosons becomes possible.

Inside the EIT medium, the hybrid superposition state is essentially a dark-state polariton (DSP) [28,29]. When a photon enters the EIT media, a supposition of photon state $\hat{E}(z, t)$ and excited magnon state $\hat{\sigma}_{12}(z, t)$ would be generated [29]:

$$\Psi(z, t) = \cos\theta \hat{E}(z, t) - \sin\theta \sqrt{N}\hat{\sigma}_{12}(z, t), \qquad (1)$$

where $\cos\theta = \Omega_c/\sqrt{\Omega_c^2 + g^2 N}$, Ω_c is the Rabi frequency of the control laser, g is the atom-field coupling constant, and N is the number of atoms. When the control laser is on,

the DSP will propagate in the medium with a slow group velocity and eventually be converted back to photons when leaving the medium. Before leaving the medium, a DSP can be converted to a pure magnon by switching off the control laser adiabatically. Therefore, by controlling the switching timing of the control laser, a hybrid BS with a temporal photonic input and a stationary magnonic input can be represented as

$$\begin{bmatrix} M_{\text{out}} \\ A_{\text{out}} \end{bmatrix} = \begin{bmatrix} t_1 & r_2 \\ r_1 & t_2 \end{bmatrix} \begin{bmatrix} M_{\text{in}} \\ A_{\text{in}} \end{bmatrix}. \qquad (2)$$

Here, M_{out} (M_{in}) and A_{out} (A_{in}) denote the magnon and photon states of output (input), respectively. $t_1 = |t_1|e^{i\phi_{1t}}$ ($r_1 = |r_1|e^{i\phi_{1r}}$) represents the transmission (reflection) coefficient of the BS for input from the magnonic port. $t_2 = |t_2|e^{i\phi_{2t}}$ ($r_2 = |r_2|e^{i\phi_{2r}}$) refers to the transmission (reflection) coefficient of the BS for input from the photonic port.

By manipulating the Rabi frequency of the control laser and optical depth (OD), the loss of the dark-state polaritons induced by atomic spontaneous emission is controllable, and eventually contributes to a tunable non-Hermitian photon-magnon interaction. Consequently, a tunable non-Hermitian beam splitter (NHBS) for these nonidentical bosons can be realized, with the non-Hermitian effect being captured by an overall phase difference $\phi_{rt} = \phi_{1r} - \phi_{2t} + \phi_{2r} - \phi_{1t}$ between the reflection and the transmission channel [30].
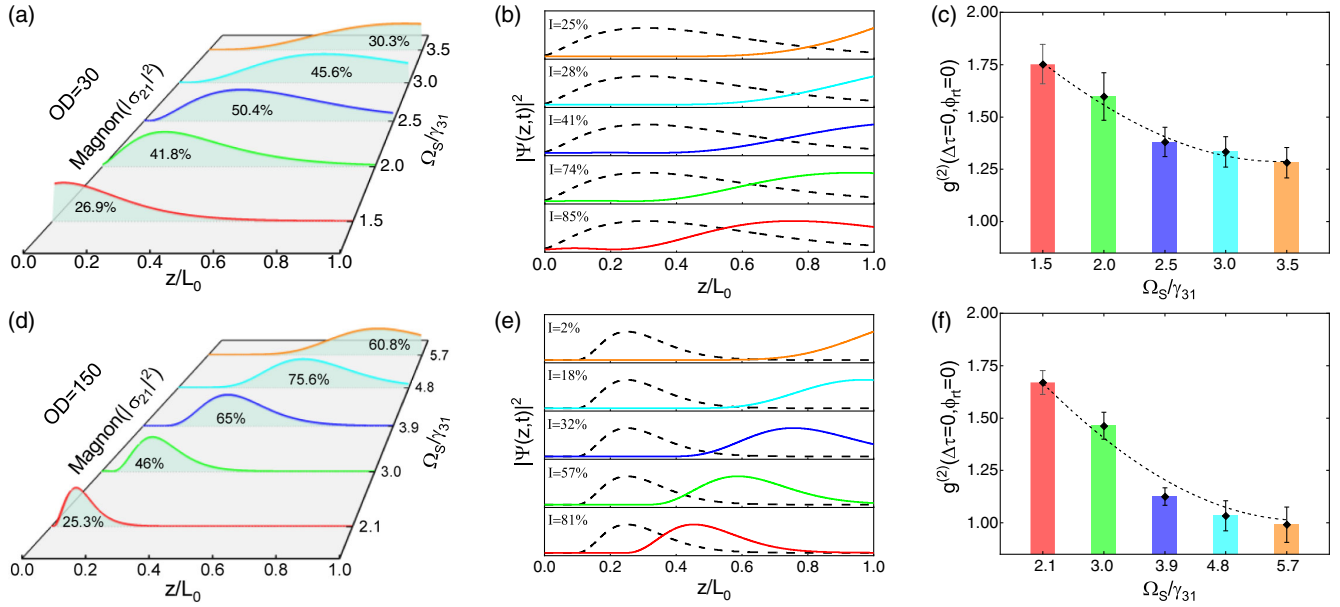
FIG. 2. The interference contrast of the magnon-photon HOM interferometer. (a),(d) Theoretically calculated magnon spatial distribution for different Ω_S. $x\%$ is the storage efficiency, and OD is the optical depth of the atomic ensemble. (b),(e) Theoretically calculated DSP spatial distribution for different Ω_S. I is the temporal envelope overlap ratio. Here, Ω_S is the same as in (a),(d) with corresponding colors. Solid line: magnon input. Dashed line: photon input. (c),(f) Experimentally measured $g^{(2)}(\Delta\tau = 0, \phi_{rt} = 0)$ with different Ω_s. z/L_0 is the normalized length of the atomic ensemble and $\gamma_{31} = 2\pi \times 3$ MHz is the dephasing rate between $|3\rangle$ and $|1\rangle$. The error bars in (c) and (f) indicate 1σ standard error from five measurements. (b) and (c) are data for OD = 30, and (e) and (f) are data for OD = 150.

For a conventional Hermitian and symmetric BS with $|t_{1,2}|^2 + |r_{1,2}|^2 = 1$, we have $\phi_{rt} = \pi$. If $|t_{1,2}|^2 + |r_{1,2}|^2 < 1$, it becomes a nonunitary BS. For the nonunitary BS, the phase difference ϕ_{rt} can be obtained as (Sec. II of Supplemental Material [31]):

$$\phi_{rt} = \arg[1 - 1/\xi] + \arg\left[\frac{\eta(\xi - 1)}{\zeta - \eta(1 - \xi)}\right], \quad (3)$$

where $\xi = e^{-|\Omega_c|^2/4(\gamma_{31} - i\Delta)\tau_p}$ and $\zeta = \frac{1}{4}|\Omega_c|^2\tau_p/\gamma_{31}$, Δ is the single photon detuning of the control laser, γ_{31} is the dephasing rate, τ_p is the temporal length of the input single photon, and η is the OD of the atomic ensemble. As shown in Fig. 1(b), there are six possible output states after the magnon-photon HOM interferometer (Sec. III of Supplemental Material [31]). Different from the Hermitian BS, with NHBS, two bosonic particles quantum interference can have an output state of $|1, 1\rangle$, where bosons behave like fermions.

As shown in Fig. 1(c), our experimental setup contains two magneto-optical traps of ^{85}Rb atoms (MOT$_1$, MOT$_2$), which serve as a heralded single photon source and an NHBS based on quantum memory, respectively. In MOT$_1$, narrow band photon pairs with a Gaussian temporal shape are generated via a spontaneous four-wave-mixing process [34–36]. First, the laser-cooled atoms are optically pumped to the lowest hyperfine level $|5S_{1/2}, F = 2\rangle$ at the

beginning of each experimental cycle. The OD of the atomic ensemble is 120 on the transition $|5S_{1/2}, F = 2\rangle \leftrightarrow |5P_{1/2}, F = 3\rangle$. Then, a pair of counterpropagating pumping laser beams (780 nm, σ^-, 14 μW) and coupling laser beams (795 nm, σ^+, 3 mW) are shone on MOT$_1$ with an angle of 2.75° to the quantization axis. A counterpropagating entangled photon pair consisting of a Stokes photon and an anti-Stokes photon (ω_{Si} and ω_{ASi}) are collected along the quantization axis. The full width at half maximum of the temporal waveform is about 100 ns. The conditional second order self-correlation function $g_e^{(2)}$ for ω_{AS} is measured to be 0.22 ± 0.03 with a Hanbury-Brown-Twiss interferometer [37], which indicates an excellent single-photon nature.

MOT$_2$ is realized with a typical EIT-based quantum memory setup [38]. Similar to MOT$_1$, the laser-cooled atoms are initialized to the Zeeman state $|5S_{1/2}, F = 2, m_F = 2\rangle$ in the experiments. The OD of the atomic ensemble can be controlled from 30 to 150 on demand. The control laser is shone on the ensemble with an angle of 1° and a beam waist of 2.3 mm. By manipulating the DSP through the control laser duration, we could realize not only the hybrid BS, but also the well-performed reversible quantum memories [38–41]. Therefore, a single magnon is prepared by storing a single photon in an EIT-based quantum memory. The magnon can then be detected after being converted back into a photon. The measured conditional second order self-correlation function $g_m^{(2)}$ for the
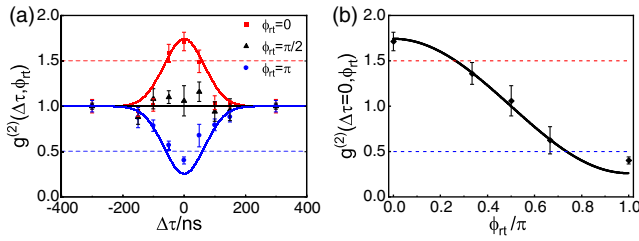
FIG. 3. Hermiticity of the magnon-photon interference. (a) The measured $g^{(2)}$ with different $\Delta\tau$. Red square: $\phi_{rt} = 0$ with $OD = 30$ and $\Delta = 0$ MHz. Blue circle: $\phi_{rt} = \pi/2$ with $OD = 66$ and $\Delta = 30$ MHz. Black triangle: $\phi_{rt} = \pi$ with $OD = 100$ and $\Delta = 60$ MHz. The solid lines are the theoretically fitted results. (b) The measured $g^{(2)}$ with different ϕ_{rt}. The solid line is the theoretically fitted result. The dashed lines are the classical limit values. The error bars represent the 1σ standard error from five measurements.

magnon prepared in MOT_2 is 0.27 ± 0.06, which shows good single particle nature.

The quantum interference experiment runs periodically with a repetition rate of 150 Hz. In each cycle, the experimental time window following the MOT loading is 0.5 ms. When a single magnon is prepared, another single photon ω_{ASi+1} produced by MOT_1 arrives at MOT_2, and the quantum interference between the magnon and photon is implemented by switching on the control laser (Ω_{BS}). During this process, there exist two overlapping DSPs inside the medium. When part of the DSP leaves the EIT medium back to photons (the photon output port), the control laser (Ω_{BS}) is switched off and the rest of the DSP is converted back to pure magnons (the magnon output port). The outputs are measured separately: the photonic output port is detected by a single photon counting module while the magnonic output is detected by switching on the control laser (Ω_R) and converting the magnons to photons. The second order magnon-photon cross-correlation after the HOM interferometer can thus be measured (Sec. IV of Supplemental Material [31]):

$$g^{(2)}(\Delta\tau, \phi_{rt}) = [1 + I(\Delta\tau)\cos(\phi_{rt})], \qquad (4)$$

where $\Delta\tau$ represents the time difference between the magnon and the photon and $I(\Delta\tau)$ represents the temporal envelope overlap ratio. The time difference $\Delta\tau$ is controllable in our experiments by manipulating the parameter Ω_{BS}. For $g^{(2)} = 2$ or 0 and $\phi_{rt} = 0$ or π, the NHBS dominates by the non-Hermitian or Hermitian nature, respectively. For $g^{(2)} = 2$, we have the $|1, 1\rangle$ magnon-photon output state, which indicates a fermionlike statistic interaction between two distinct bosons.

For an ideal HOM interference, $I(\Delta\tau) = 1$ is expected when $\Delta\tau = 0$. However, completely overlapping two DSPs in the EIT medium is challenging. In our work, we could maximize the overlap by tuning Ω_S to optimize the interference contrast. The spatial distribution of the magnon over the atomic medium is calculated in the storage process, as shown in Figs. 2(a) and 2(d). We also numerically simulate the evolution of both DSPs when another photon enters the EIT medium. As shown in Figs. 2(b) and 2(e), the overlap ratio described by the normalized overlap integration between two DSPs is determined by the initial position of the prepared magnon. The above theoretical results are calculated through the optical Bloch equations (Eq. S6 in Supplemental Material [31]). The maximum overlap ratio can be obtained by choosing a proper Ω_S in the storage process. The splitting ratio $|t_1/r_1|(|t_2/r_2|)$ is controlled by the switching off time of the Ω_{BS}. In the experiment, Ω_{BS} is switched off at the center of the two DSPs, thus $|t_1/r_1| \approx |r_2/t_2|$. As shown in Figs. 2(c) and 2(f), the second order cross-correlation $g^{(2)}$ is measured with different Ω_S and different ODs. High interference contrast can be realized with different ODs by controlling Ω_S. The maximum $g^{(2)} = 1.75 \pm 0.09$ is realized in the experiment, which is limited by the maximum achievable overlap ratio.

With $|t_1|^2 = 0.15$, $|r_1|^2 = 0.20$, $|t_1|^2 + |r_1|^2 \approx 0.35$, $|t_2|^2 = 0.26$, $|r_2|^2 = 0.22$, and $|t_2|^2 + |r_2|^2 \approx 0.48$, we
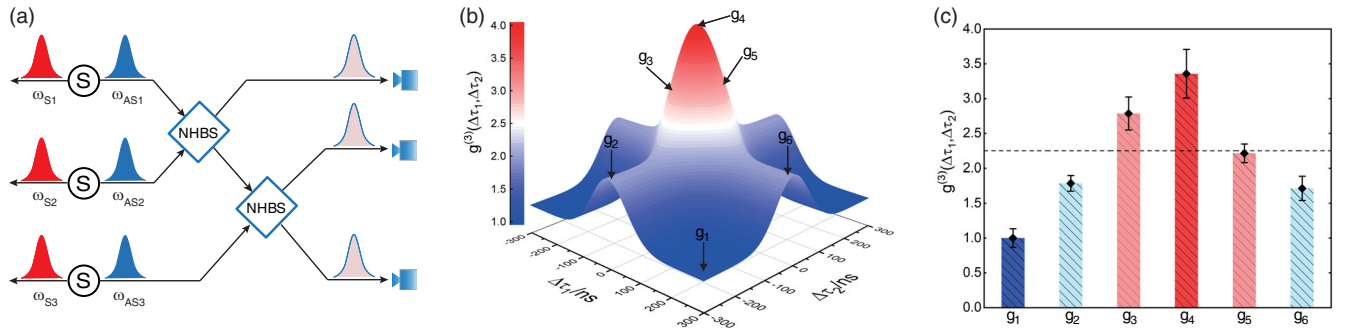

FIG. 4. Three-photon interference. (a) Experimental scheme. S is the paired photon source (ω_{Si} and ω_{ASi}) and NHBS is the quantum memory based non-Hermitian beam splitter. (b) The theoretically calculated $g^{(3)}(\Delta\tau_1, \Delta\tau_2)$ with different time delays $\Delta\tau_1$ and $\Delta\tau_2$. (c) The experimental results of $g^{(3)}(\Delta\tau_1, \Delta\tau_2)$, corresponding to the points signed in (b). The dashed line is the classical limit value. The error bars in (c) indicate 1σ standard error from five measurements.

observed the optimal interference contrast. The loss of the magnon is determined by Ω_S in the storage process. The loss of the photon is determined by Ω_{BS} in the interference process. Under these conditions, the non-Hermicity of the BS can be further tuned by controlling ϕ_{rt} from 0 to π according to Eq. (2). With an acousto-optic modulator, the detuning Δ of the control laser can be arbitrarily controlled and thus change the relative phase ϕ_{rt} from 0 to π, which indicates the transition from a non-Hermitian BS to a Hermitian BS. This relative phase usually shows no significant effect on single particle interference but fundamentally affects two-particle interference. Here, we experimentally demonstrate that, by tuning the non-Hermicity of the BS, we can transition the bosonic HOM interference to the fermionic HOM interference between two bosons. As shown in Fig. 3, the HOM interference bump and dip are observed in the experiment with different Δ. The maximum $g^{(2)} = 1.71$ of the bump and the minimum $g^{(2)} = 0.4$ of the dip are measured, which significantly violate the respective classical limit of the second order cross-correlation of 0.5 and 1.5 [31,42]. In our experiment, loss is kept stable by adjusting the resonant OD for different Δ. Our results agree well with theoretical simulations and indicate that a quantum two-particle interference is realized.

We next utilize our NHBS to realize three-photon interference. When $\phi_{rt} = 0$, the third-order cross-correlation of three output photons can be described [31] by

$$g^{(3)}(\Delta\tau_1, \Delta\tau_2) = [1 + I(\Delta\tau_1)][1 + I(\Delta\tau_2)], \qquad (5)$$

where $\Delta\tau_1$ and $\Delta\tau_2$ represent the time difference between the first-second and second-third photons, respectively. Three photons sequentially generated from a single photon source are guided one by one into the quantum memory based on NHBS, as shown in Fig. 4(a). With $\phi_{rt} = 0$, three-photon antibunching effects can be observed in three output ports [Fig. 4(b)]. In an ideal three-photon NHBS interference, the third order cross-correlation function $g^{(3)}$ of photons in output ports is expected to be 4 while the classical threshold is 1.5^2, see Supplemental Material [31]. As shown in Fig. 4(c), we achieve a maximal $g^{(3)}$ of 3.36 ± 0.35 with $\Delta\tau_1 = \Delta\tau_2 = 0$, which shows that multiparticle interference works in the quantum regime. In this interference scheme, a postselected triphoton state of $|1, 1, 1\rangle$ can be produced in a heralded manner, and it shows a fermion-like statistic behavior.

In conclusion, we have demonstrated quantum interference between nonidentical bosonic particles (a single magnon and a single photon) using an atomic hybrid BS with tunable splitting ratio, loss, and non-Hermicity. In our magnon-photon quantum interferometer, both bosonic bunching and fermionic antibunching are observed by controlling the non-Hermicity of the hybrid magnon-photon beam splitter. Furthermore, multiparticle interference that simulates the behavior of three fermions by three input photons is realized. Our result validates and deepens the understanding of quantum interference and could stimulate further experimental and theoretical investigations of the quantum effects between distinction bosons or fermions. Our work also unveils the cold atom quantum memory as a versatile platform, which has the advantages of a long coherence time, multiple polariton modes, and fully controllable parameters of the generalized beam splitter. The cold atom quantum memory has potential for studying fundamental quantum mechanics and realizing innovative quantum devices for linear optical quantum computation, boson sampling, and quantum walk [43–45].

K. Su and Y. Zhong contributed equally.

———

[*]yunfeiwang2014@126.com
[†]yanhui@scnu.edu.cn
[‡]slzhu@scnu.edu.cn

[1] C. K. Hong, Z. Y. Ou, and L. Mandel, Measurement of Subpicosecond Time Intervals between Two Photons by Interference, Phys. Rev. Lett. **59**, 2044 (1987).

[2] A. Aspuru-Guzik and P. Walther, Photonic quantum simulators, Nat. Phys. **8**, 285 (2012).

[3] M. Tillmann, B. Dakić, R. Heilmann, S. Nolte, A. Szameit, and P. Walther, Experimental boson sampling, Nat. Photonics **7**, 540 (2013).

[4] A. N. Vetlugin, R. Guo, C. Soci, and N. I. Zheludev, Anti-Hong-Ou-Mandel effect with entangled photons, arXiv:2105.05444.

[5] M. C. Tichy, M. Tiersch, F. Mintert, and A. Buchleitner, Many-particle interference beyond many-boson and many-fermion statistics, New J. Phys. **14**, 093015 (2012).

[6] F. Bouchard, A. Sit, Y. W. Zhang, R. Fickler, F. M. Miatto, Y. Yao, F. Sciarrino, and E. Karimi, Two-photon interference: The Hong-Ou-Mandel effect, Rep. Prog. Phys. **84**, 012402 (2021).

[7] J. Li, M. T. Zhou, B. Jing, X. J. Wang, S. J. Yang, X. Jiang, K. Molmer, X. H. Bao, and J. W. Pan, Hong-Ou-Mandel Interference between Two Deterministic Collective Excitations in an Atomic Ensemble, Phys. Rev. Lett. **117**, 180501 (2016).

[8] J. S. Fakonas, H. Lee, Y. A. Kelaita, and H. A. Atwater, Two-plasmon quantum interference, Nat. Photonics **8,** 317 (2014).

[9] R. W. Heeres, L. P. Kouwenhoven, and V. Zwiller, Quantum interference in plasmonic circuits, Nat. Nanotechnol. **8,** 719 (2013).

[10] R. Lopes, A. Imanaliev, A. Aspect, M. Cheneau, D. Boiron, and C. I. Westbrook, Atomic Hong-Ou-Mandel experiment, Nature (London) **520,** 66 (2015).

[11] A. M. Kaufman, B. J. Lester, C. M. Reynolds, M. L. Wall, M. Foss-Feig, K. R. A. Hazzard, A. M. Rey, and C. A. Regal, Two-particle quantum interference in tunnel-coupled optical tweezers, Science **345,** 306 (2014).

[12] E. Knill, R. Laflamme, and G. J. Milburn, A scheme for efficient quantum computation with linear optics, Nature (London) **409,** 46 (2001).

[13] P. Kok, W. J. Munro, K. Nemoto, T. C. Ralph, J. P. Dowling, and G. J. Milburn, Linear optical quantum computing with photonic qubits, Rev. Mod. Phys. **79,** 135 (2007).

[14] R. Okamoto, J. L. O'Brien, H. F. Hofmann, and S. Takeuchi, Realization of a Knill-Laflamme-Milburn controlled-NOT photonic quantum circuit combining effective optical non-linearities, Proc. Natl. Acad. Sci. U.S.A. **108,** 10067 (2011).

[15] J. W. Pan, Z. B. Chen, C. Y. Lu, H. Weinfurter, A. Zeilinger, and M. Zukowski, Multiphoton entanglement and interferometry, Rev. Mod. Phys. **84,** 777 (2012).

[16] L. M. Duan, M. D. Lukin, J. I. Cirac, and P. Zoller, Long-distance quantum communication with atomic ensembles and linear optics, Nature (London) **414,** 413 (2001).

[17] N. Sangouard, C. Simon, H. de Riedmatten, and N. Gisin, Quantum repeaters based on atomic ensembles and linear optics, Rev. Mod. Phys. **83,** 33 (2011).

[18] Toshiki Kobayashi, Rikizo Ikuta, Shuto Yasui, Shigehito Miki, Taro Yamashita, Hirotaka Terai, Takashi Yamamoto, Masato Koashi, and Nobuyuki Imoto, Frequency-domain Hong-Ou-Mandel interference, Nat. Photonics **10,** 441 (2016).

[19] X. Wang, J. Wang, Z. Ren, R. Wen, C. L. Zou, G. A. Siviloglou, and J. F. Chen, Quantum Interference between Photons and Single Quanta of Stored Atomic Coherence, Phys. Rev. Lett. **128,** 083605 (2022).

[20] B. Vest, M. C. Dheur, E. Devaux, A. Baron, E. Rousseau, J. P. Hugonin, J. J. Greffet, G. Messin, and F. Marquier, Anti-coalescence of bosons on a lossy beam splitter, Science **356,** 1373 (2017).

[21] Q. W. Li, W. Bao, Z. Y. Nie, Y. Xia, Y. H. Xue, Y. Wang, S. Yang, and X. Zhang, A non-unitary metasurface enables continuous control of quantum photon-photon interactions from bosonic to fermionic, Nat. Photonics **15,** 267 (2021).

[22] M. Ehrhardt, M. Heinrich, and A. Szameit, Observation-dependent suppression and enhancement of two-photon coincidences by tailored losses, Nat. Photonics **16,** 191 (2022).

[23] T. Roger, S. Restuccia, A. Lyons, D. Giovannini, J. Romero, J. Jeffers, M. Padgett, and D. Faccio, Coherent Absorption of N00N States, Phys. Rev. Lett. **117,** 023601 (2016).

[24] K.-J. Boller, A. Imamoğlu, and S. E. Harris, Observation of Electromagnetically Induced Transparency, Phys. Rev. Lett. **66,** 2593 (1991).

[25] C. Liu, Z. Dutton, C. H. Behroozi, and L. V. Hau, Observation of coherent optical information storage in an atomic medium using halted light pulses, Nature (London) **409,** 490 (2001).

[26] D. F. Phillips, A. Fleischhauer, A. Mair, R. L. Walsworth, and M. D. Lukin, Storage of Light in Atomic Vapor, Phys. Rev. Lett. **86,** 783 (2001).

[27] M. D. Lukin, Colloquium: Trapping and manipulating photon states in atomic ensembles, Rev. Mod. Phys. **75,** 457 (2003).

[28] M. Fleischhauer and M. D. Lukin, Quantum memory for photons: Dark-state polaritons, Phys. Rev. A **65,** 022314 (2002).

[29] M. Fleischhauer and M. D. Lukin, Dark-State Polaritons in Electromagnetically Induced Transparency, Phys. Rev. Lett. **84,** 5094 (2000).

[30] R. Wen, C. L. Zou, X. Zhu, P. Chen, Z. Y. Ou, J. F. Chen, and W. Zhang, Non-Hermitian Magnon-Photon Interference in an Atomic Ensemble, Phys. Rev. Lett. **122,** 253602 (2019).

[31] See Supplemental Material at http://link.aps.org/supplemental/10.1103/PhysRevLett.129.093604 for detailed theoretical model and calculations, which includes Refs. [32,33].

[32] S. M. Barnett, J. Jeffers, A. Gatti, and R. Loudon, Quantum optics of lossy beam splitters, Phys. Rev. A **57,** 2134 (1998).

[33] Vlatko Balić, Danielle A. Braje, Pavel Kolchin, G. Y. Yin, and S. E. Harris, Generation of Paired Photons with Controllable Waveforms, Phys. Rev. Lett. **94,** 183601 (2005).

[34] J. F. Li, Y. F. Wang, K. Y. Su, K. Y. Liao, S. C. Zhang, H. Yan, and S. L. Zhu, Generation of Gaussian-shape single photons for high efficiency quantum storage, Chin. Phys. Lett. **36,** 074202 (2019).

[35] L. W. Zhao, X. X. Guo, Y. Sun, Y. M. Su, M. M. T. Loy, and S. W. Du, Shaping the Biphoton Temporal Waveform with Spatial Light Modulation, Phys. Rev. Lett. **115,** 193601 (2015).

[36] K. Y. Liao, H. Yan, J. Y. He, S. W. Du, Z. M. Zhang, and S. L. Zhu, Subnatural-Linewidth Polarization-Entangled Photon Pairs with Controllable Temporal Length, Phys. Rev. Lett. **112,** 243602 (2014).

[37] P. Grangier, G. Roger, and A. Aspect, Experimental evidence for a photon anticorrelation effect on a beam splitter: A new light on single-photon interferences, Europhys. Lett. **1,** 173 (1986).

[38] Y. F. Wang, J. F. Li, S. C. Zhang, K. Y. Su, Y. R. Zhou, K. Y. Liao, S. W. Du, H. Yan, and S. L. Zhu, Efficient quantum memory for single-photon polarization qubits, Nat. Photonics **13,** 346 (2019).

[39] Y. F. Hsiao, P. J. Tsai, H. S. Chen, S. X. Lin, C. C. Hung, C. H. Lee, Y. H. Chen, Y. F. Chen, I. A. Yu, and Y. C. Chen, Highly Efficient Coherent Optical Memory Based on Electromagnetically Induced Transparency, Phys. Rev. Lett. **120,** 183602 (2018).

[40] P. Vernaz-Gris, K. Huang, M. T. Cao, A. S. Sheremet, and J. Laurat, Highly-efficient quantum memory for polarization qubits in a spatially-multiplexed cold atomic ensemble, Nat. Commun. **9,** 363 (2018).

[41] K. Su, Y. Wang, S. Zhang, Z. Kong, Y. Zhong, J. Li, H. Yan, and S. L. Zhu, Synchronization and phase shaping of single

photons with high-efficiency quantum memory, Chin. Phys. Lett. **38**, 094202 (2021).

[42] Z. Q. Ren, R. Wen, and J. F. Chen, Photon coalescence in a lossy non-Hermitian beam splitter, Chin. Phys. Lett. **37**, 084203 (2020).

[43] H. S. Zhong, H. Wang, Y. H. Deng, M. C. Chen, L. C. Peng, Y. H. Luo, J. Qin, D. Wu, X. Ding, Y. Hu *et al.*, Quantum computational advantage using photons, Science **370**, 1460 (2020).

[44] J. C. F. Matthews, K. Poulios, J. D. A. Meinecke, A. Politi, A. Peruzzo, N. Ismail, K. Wörhoff, M. G. Thompson, and J. L. O'Brien, Observing fermionic statistics with photons in arbitrary processes, Sci. Rep. **3**, 1539 (2013).

[45] L. Sansoni, F. Sciarrino, G. Vallone, P. Mataloni, A. Crespi, R. Ramponi, and R. Osellame, Two-Particle Bosonic-Fermionic Quantum Walk via Integrated Photonics, Phys. Rev. Lett. **108**, 010502 (2012).